

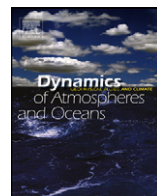


ELSEVIER

Contents lists available at SciVerse ScienceDirect

Dynamics of Atmospheres and Oceans

journal homepage: www.elsevier.com/locate/dynatmoce



Impact of remote forcing, model resolution and bathymetry on predictions of currents on the shelf



Igor Shulman^{a,*}, Steven R. Ramp^b, Stephanie Anderson^a,
E. Joseph Metzger^a, Peter Sakalaukus^a

^a Oceanography Division, Naval Research Laboratory, Stennis Space Center, MS, United States

^b Soliton Ocean Services, Inc., Carmel Valley 93924, CA, United States

ARTICLE INFO

Article history:

Received 14 November 2012

Received in revised form 28 February 2013

Accepted 1 March 2013

Available online 14 March 2013

Keywords:

Coastal circulation

Ocean modeling and prediction

Coastally-trapped waves

USA/California/Monterey Bay

ABSTRACT

Impacts of remote forcing, model resolution and bathymetry on current predictions at two moorings located on the shelf of the Monterey Bay area are investigated. We consider three Monterey Bay model configurations which differ in resolution and bathymetry representation, and we specify open boundary conditions for these three configurations from two larger scale models, which have different accuracy in the representation of the remote forcing (in the form of poleward propagating along the coast coastally-trapped Kelvin type waves).

Comparisons of correlations between observed and model currents as well as visual comparisons show that the most critical element in reproducing currents on the shelf is accurate representation of the remote forcing. Our results also show that accurate representation of bathymetry is the second most critical factor in reproducing observed currents.

Published by Elsevier B.V.

1. Introduction

The objectives of the August 2006 field experiment, called Adaptive Sampling and Prediction (ASAP), were mostly focused on the study of the properties of the upwelling center at Año Nuevo

* Corresponding author at: Naval Research Laboratory, Building 1009, Stennis Space Center, MS 39529, United States.
Tel.: +1 228 6885646.

E-mail address: igor.shulman@nrlssc.navy.mil (I. Shulman).

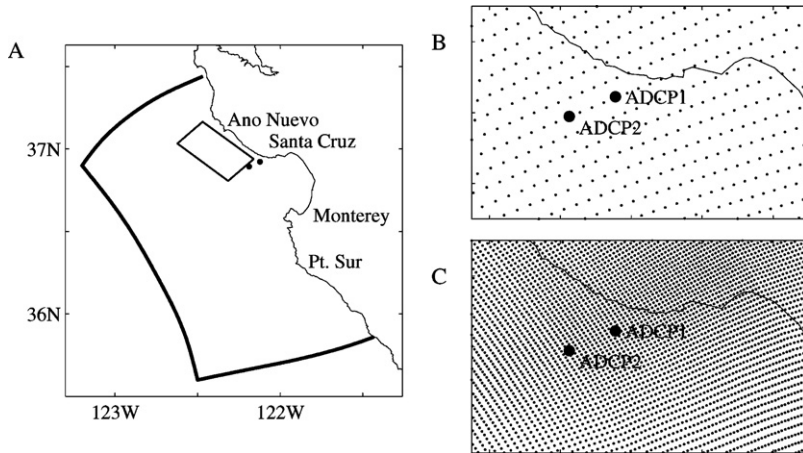


Fig. 1. (A) The Monterey Bay modeling domain with locations of ADCP1, ADCP2 and the ASAP glider sampling domain to the north of the ADCPs. (B) Grid resolution around ADCPs for MBS1 and MBS2 configurations. (C) Grid resolution around ADCPs for MBS3.

to the north of the Monterey Bay (Ramp et al., 2011; Leonard et al., 2010; Shulman et al., 2010). For this reason, the extensive sampling was conducted inside of an approximately 1000 km² box (Fig. 1), where a fleet of ten gliders under autonomous control were deployed for a period of 30 days, and research aircraft observed the fluxes through the sea surface. Two bottom-mounted acoustic Doppler current profilers (ADCPs) were deployed about 6.5 km apart to the south of the ASAP box (Fig. 1), to monitor the currents over the continental shelf (Ramp et al., 2011). Despite being only 6.5 km apart, ADCP moorings 1 and 2 responded differently to the sequence of upwelling favorable winds separated by brief relaxations. Predictions from three simulations of the Monterey Bay area based on the Harvard Ocean Prediction System (HOPS), the Regional Ocean Modeling System (ROMS), and the Navy Coastal Ocean Model (NCOM) were quantitatively compared with the observed currents at the two moorings' locations on the shelf (Ramp et al., 2011). All three model simulations, with well-established performance at larger space and time scales, had difficulty reproducing the current variability in this small sample region around mooring locations (with relatively better performance in the alongshore than a cross-shore directions). It was speculated that one of the reasons is that model open boundary conditions could not capture remote forcing in the form of alongshore pressure gradient forces or coastally-trapped waves, which propagate from south to north with the coast on the right in this region. Other considered reasons were that very high horizontal resolution (at least 0.5 km) and more accurate representation of bathymetry are needed to reproduce currents variability on the continental shelf (based on relatively better performance of the finer resolution simulation based on the HOPS system). Because the three considered modeling systems had so many differences in specification of open boundary conditions, data assimilation schemes, bathymetry, horizontal and vertical resolution, parameterization, and ways of applying atmospheric conditions, it was difficult to sort out reasons for model difficulties in reproducing currents in the framework of the Ramp et al. (2011) study.

The objective of this short follow up to Ramp et al. (2011) paper is to use one model (NCOM) and identify the impacts of remote forcing, model resolution and bathymetry representation on the model current predictions on the shelf. For doing these we consider three NCOM configurations which differ in resolution and bathymetry representation and we specify open boundary conditions for these three configurations from two different larger scale models, which have different accuracy in the representation of the remote forcing (the coastally-trapped Kelvin type waves).

The structure of the paper is as follows: Section 2 describes observations, Monterey Bay model configurations and open boundary conditions used in this study. The design of model runs is described in Section 3, Section 4 presents results of experiments and Section 5 is devoted to conclusions and discussions.

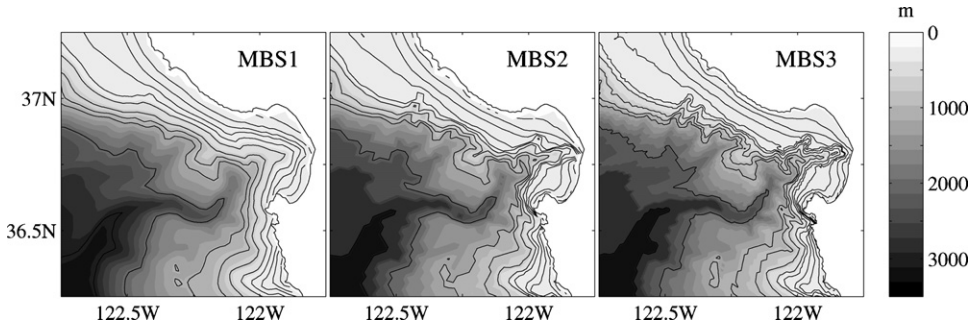


Fig. 2. Bathymetry for model configurations MBS1–MBS3.

2. Methods

2.1. ADCP data

A comprehensive description of ADCP data is presented in Ramp et al. (2011). Here we provide a brief of this description. The moorings deployed for the August 2006 experiment consisted of two 300 kHz acoustic Doppler current profilers (ADCPs) in trawl-resistant bottom mounts (TRBMs) located 6.55 km apart. ADCP 1 was located at $36^{\circ} 55.336' N$, $122^{\circ} 07.344' W$, 54 m depth, and ADCP 2 was located at $36^{\circ} 53.683' N$, $122^{\circ} 11.244' W$, 92 m depth (Fig. 1). The data were sampled in 4-m bins from the bottom to the surface; however the uppermost 3 bins (12 m) were lost due to side-lobe reflection. The basic 1-min time series were obtained by ensemble averaging 60 1-s pings in the instrument. Subsequent averaging and filtering to separate the frequency bands of interest were accomplished in the laboratory. An inverse-Fourier truncation method was used to remove internal waves with periods of five hours or less. The residual time series were filtered again with the half-power point at 33 h (Beardsley et al., 1985) to separate the tidal and inertial motions from the wind forced, mesoscale, and mean currents.

2.2. The NCOM Monterey Bay model configurations

The NCOM is a primitive-equation, 3D, hydrostatic model. It uses the Mellor-Yamada level 2.5 turbulence closure scheme, and the Smagorinsky formulation for horizontal mixing (Martin, 2000).

Three NCOM configurations of the Monterey Bay area are used in this study. All three set ups cover the same domain (shown in Fig. 1). They are all forced with surface fluxes from the Coupled Ocean and Atmospheric Mesoscale Prediction System (COAMPS) (Doyle et al., 2009) atmospheric model at 3 km horizontal resolution. The bathymetry with the horizontal resolution of approximately 0.01° (~ 1 km) was interpolated to the centers of the horizontal grids to derive depths for all of the described below three model configurations.

2.2.1. First Monterey Bay model configuration (MBS1)

The first configuration is the model set up used in Ramp et al. (2011). This configuration is noted as MBS1. The MBS1 has a curvilinear orthogonal horizontal grid with resolution ranging from 1 to 4 km, near the ADCPs the resolution is about $1.5 \text{ km} \times 2.5 \text{ km}$ (Fig. 1B). There are 30 sigma-coordinate vertical levels. Because of the sigma-coordinate vertical system, the bathymetry has to be smoothed to minimize problems associated with sigma-coordinates over steep topography (Haney, 1991). The bathymetry for the MBS1 is shown in Fig. 2.

2.2.2. Second Monterey Bay model configuration (MBS2)

The second configuration (noted by MBS2) has the same horizontal resolution as the MBS1, but with a different vertical coordinate system. MBS2 has 40 hybrid (sigma-z) levels total, 19 sigma layers from

the surface down to 138-m depth and 21 z-levels between 138 m and bottom. In this case, with z levels on the bottom, there is no need to smooth bathymetry, and bathymetry used for MBS2 configuration is shown in Fig. 2.

2.2.3. Third Monterey Bay model configuration (MBS3)

The third configuration (noted by MBS3) has a finer resolution horizontal grid in comparison to MBS1 and MBS2. The grid is also a curvilinear orthogonal grid with a resolution of $0.4 \text{ km} \times 1.5 \text{ km}$, and near the ADCPs the resolution is about $0.5 \text{ km} \times 0.7 \text{ km}$ (Fig. 1C). The vertical grid consists of 49 hybrid (sigma-z) levels total, 24 sigma layers from the surface down to 146-m depth and 25 z-levels between 146 m and bottom. The bathymetry for MBS3 is shown in Fig. 2.

2.3. Open boundary data and remote forcing

Two larger scale model's outputs are used to provide boundary conditions for the Monterey Bay model configurations described in Section 2.2. The first model is the NCOM-based regional model of the California Current (NCOM CCS, Shulman et al., 2007). The NCOM CCS has a horizontal resolution of about 9 km and uses the same 40-layer, hybrid vertical grid used in the MBS2 set up. The NCOM CCS domain extends from 30° N to 49° N of latitude and from the coast to 135° W of longitude. The NCOM CCS model is forced with atmospheric products derived from the COAMPS predictions (Doyle et al., 2009). The NCOM CCS assimilates three-dimensional temperature and salinity observations derived from the Modular Ocean Data Assimilation System (MODAS; Fox et al., 2002). Open boundary conditions for the NCOM CCS model are derived from global NCOM model (Rhodes et al., 2002; Barron et al., 2004).

The second larger-scale model is the global model based on the Hybrid Coordinate Ocean Model (HYCOM) (Chassignet et al., 2009; Metzger et al., 2010). The model has $\sim 1/12^\circ$ horizontal resolution and 32 vertical layers. It uses the Navy Coupled Ocean Data Assimilation (NCODA) system for assimilation of satellite surface temperature, as well as available in situ vertical temperature and salinity profiles from XBTs, Argo floats, moored buoys and gliders from the Global Ocean Data Assimilation Experiment (GODAE) data set (Cummings, 2005; Cummings et al., 2009). The model is forced with atmospheric fluxes from the Navy Global Atmospheric Prediction System (NOGAPS; Rosmond et al., 2002).

In Ramp et al. (2011, Fig. 12), the comparison of sea surface height (SSH) anomalies along the California coast estimated from the NCOM CCS and the global HYCOM with the coastal SSH observations for May–September of 2006 are presented. Both models and observations show strong positive SSH anomalies during August 2006 (Ramp et al., 2011; Shulman et al., 2010). Both models also show that these anomalies were propagating poleward at $1\text{--}3 \text{ m s}^{-1}$, which is in agreement with previous estimates of phase seed for the first baroclinic coastally-trapped Kelvin wave (e.g. Chelton and Davis, 1982; Denbo and Allen, 1987; Spillane et al., 1987; Zamudio et al., 2008, 2011). These anomalies therefore represent remote forcing which will impact the Monterey Bay area, and a smaller region around ADCP 1 and 2 on the shelf. Comparing the model SSH with the observed SSH at Monterey and San Diego tide stations shows that the NCOM CCS underestimated these propagating anomalies with respect to both the observations and HYCOM, which closely-tracked the observed fluctuations (see Fig. 3 which is Fig. 12 of Ramp et al., 2011, and reproduced here for clarity presentation). Therefore, the use of the HYCOM output as open boundary conditions for the Monterey Bay model (configurations MBS1–3 in Section 2.2) will provide more accurate representation of remote forcing on the southern open boundary in comparison to using the NCOM CCS.

Sea surface elevations and vertically averaged velocities (barotropic information) from the Monterey Bay model and larger scale model (NCOM CCS or HYCOM) are coupled through the Flather (1976) boundary condition:

$$u_n = u_n^o + \left(\frac{g}{H}\right)^{1/2} (\eta - \eta^o) \quad (1)$$

where η and u_n are the Monterey Bay model (configurations MS1–3, Section 2.2) sea surface height and the vertically averaged normal component of velocity on the open boundary, η^o and u_n^o are the

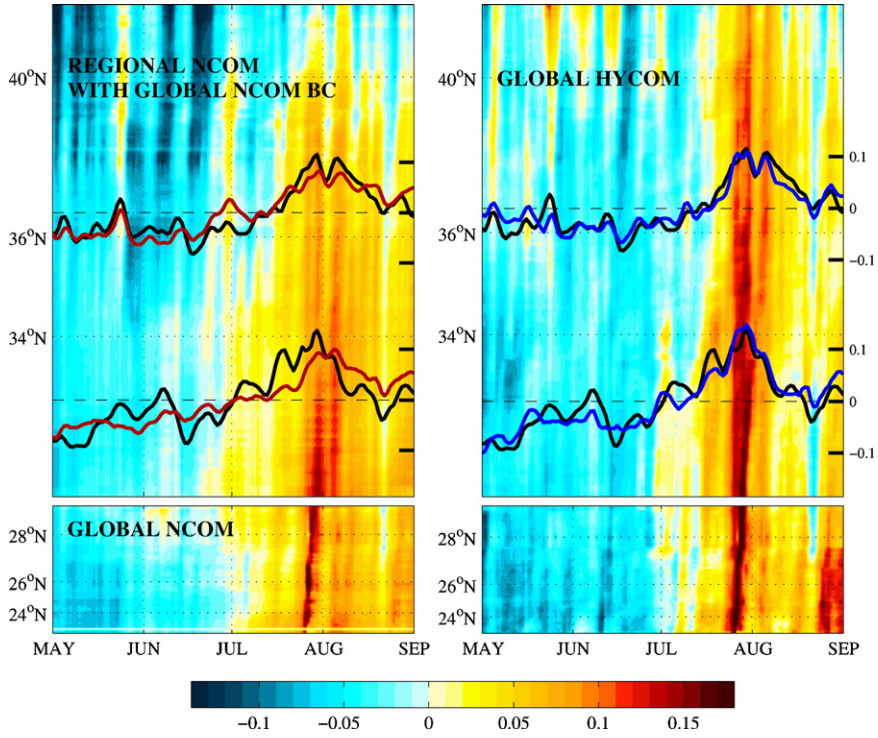


Fig. 3. Sea surface height (SSH) anomalies from 24° N to 40° N as computed by (left panel) the regional NCOM CCS model with global NCOM boundary conditions and (right panel) global HYCOM. The observed SSH from coastal sea level observations at Monterey (36° 36' N) and San Diego (32° 43' N) are included as the heavy black lines. Time series at the same locations sub-sampled from the two different model configurations are shown as the red (NCOM) and blue (HYCOM) lines respectively.

sea surface height and the vertically averaged normal component of velocity from larger scale model (NCOM CCS or HYCOM). The open boundary condition (1) represents a radiation condition on differences between the Monterey Bay and larger scale model sea level elevations and transports. The baroclinic coupling consists of using the vertical structure of velocity, temperature, and salinity from the larger scale model in specification of the vertical distributions of the Monterey Bay model.

3. Experiments design

To investigate the impact of remote forcing, model resolution and bathymetry on coastal model predictions of currents on the shelf, we conducted six experiments using all three Monterey model set ups (MBS1–3, described in Section 2.2) with open boundary conditions derived from two larger-scale models (NCOMCCS and HYCOM) described in Section 2.3. Attributes of six runs are listed in Table 1.

Table 1
Monterey Bay model runs.

Runs	OBCS	Model	Vertical grid	Bathymetry	Horizontal resolution
1	NCOM CCS	MBS1	Sigma	Smoothed	1.5 km × 2.5 km
2	NCOM CCS	MBS2	Hybrid	Non-smoothed	1.5 km × 2.5 km
3	NCOM CCS	MBS3	Hybrid	Non-smoothed	0.5 km × 0.7 km
4	HYCOM	MBS1	Sigma	Smoothed	1.5 km × 2.5 km
5	HYCOM	MBS2	Hybrid	Non-smoothed	1.5 km × 2.5 km
6	HYCOM	MBS3	Hybrid	Non-smoothed	0.5 km × 0.7 km

Run 1 was conducted with the MBS1 configuration (Section 2.2). The run was initialized on 27 July 2006 00Z from the NCOM CCS model, and run until 1 September 2006 00Z using the NCOM CCS as open boundary conditions.

Run 2 was conducted with the MBS2 configuration (Section 2.2). The run also was initialized on 27 July 2006 00Z from the NCOM CCS model, and run until 1 September 2006 00Z using the same open boundary conditions as in Run 1.

Run 3 was conducted with the MBS3 configuration. As with Runs 1 and 2, Run 3 also was initialized on 27 July 2006 00Z from the NCOM CCS model, and run until 1 September 2006 00Z using NCOM CCS as open boundary conditions.

Comparisons of Runs 1–3 demonstrate the impact of resolution and bathymetry on current predictions in the case when open boundary conditions (NCOM CCS) underestimate remote forcing in the form of poleward propagating coastally-trapped Kelvin waves (Section 2.3).

Run 4–6 are analogs of Runs 1–3 in the way that MBS1–MBS3 configurations are used as in Runs 1–3 (see Table 1). The difference is that Runs 4–6 were initialized from the global HYCOM model on 27 July 2006 00Z and were run with the open boundary conditions from HYCOM.

Therefore, comparisons of Runs 1–3 with corresponding Runs 4–6 demonstrate the impact of remote forcing (in the form of poleward propagating coastally-trapped Kelvin waves) on the model currents predictions on the shelf.

The magnitudes of complex correlation coefficients and angular displacements between ADCP currents and model currents were used for evaluating the above model runs.

The magnitude R of the complex correlation coefficient and the angular displacement θ between the ADCP and the model currents for a particular depth are estimated using the approach outlined in Kundu (1976). The magnitude R is estimated as:

$$R = \sqrt{Re^2 + Im^2} \quad (2)$$

where

$$Re = \frac{\sum_t (u_t^o u_t^m + v_t^o v_t^m)}{\sqrt{\sum_t ((u_t^o)^2 + (v_t^o)^2) \sum_t ((u_t^m)^2 + (v_t^m)^2)}},$$

$$Im = \frac{\sum_t (u_t^o v_t^m - v_t^o u_t^m)}{\sqrt{\sum_t ((u_t^o)^2 + (v_t^o)^2) \sum_t ((u_t^m)^2 + (v_t^m)^2)}}.$$

The corresponding angular displacement θ , which is also called the phase angle, is computed according to:

$$\theta = \tan^{-1} \frac{\sum_t (u_t^o v_t^m - v_t^o u_t^m)}{\sum_t (u_t^o u_t^m + v_t^o v_t^m)} \quad (3)$$

where u_t^m, v_t^m are the demeaned east–west and north–south model velocity components, respectively, and u_t^o, v_t^o are the demeaned east–west and north–south observed velocity components, respectively. The angular displacement θ gives the average counterclockwise angle difference between model and observed velocity vectors. The value of θ is only meaningful if R is significant. Correlations are estimated over a 28-day period (August 2–30 of 2006) using hourly model and observed data passing through a 33-h low-pass-filter. Therefore, the actual number of degrees of freedom is less or equal to $28 \times 24/33 \approx 20$. With 20 degrees of freedom, a correlation of 0.44 is significant at 95% confidence level (see, for example Wilks, 1995). Therefore, correlations less than 0.44 should be considered as insignificant.

4. Results

Tables 2 and 3 present complex correlations and angular displacements between observed and model currents. Three ADCP bins are chosen: near-surface (12–16 m), mid-depth (28–32, 48–52)

Table 2

Complex correlations and angular displacements between model-predicted and observed currents at ADCP1. Statistically significant correlations and corresponding angular displacements are in bold.

Depth	12–16 m		28–32		50–54	
	<i>R</i>	θ	<i>R</i>	θ	<i>R</i>	θ
Run 1	0.1	3.5	0.12	–135.2	0.13	123.2
Run 2	0.19	–31.9	0.13	–66.0	0.04	135.2
Run 3	0.11	109.9	0.06	–26.9	0.14	59.6
Run 4	0.39	–19.8	0.55	–15.5	0.26	–7.6
Run 5	0.66	–12.1	0.79	–6.7	0.70	–0.8
Run 6	0.57	–15.6	0.64	–7.0	0.34	–4.0

Table 3

Complex correlations and angular displacements between model-predicted and observed currents at ADCP2. Statistically significant correlations and corresponding angular displacements are in bold.

Depth	12–16 m		48–52		88–92	
	<i>R</i>	θ	<i>R</i>	θ	<i>R</i>	θ
Run 1	0.32	175.5	0.28	160.2	0.08	150.2
Run 2	0.28	43.3	0.21	23.1	0.34	–18.9
Run 3	0.21	101.2	0.21	142.2	0.24	5.2
Run 4	0.63	–13.3	0.62	–13.5	0.45	4.2
Run 5	0.83	–4.8	0.77	–6.9	0.64	–3.4
Run 6	0.40	–21.2	0.4	–32.3	0.20	–28.8

and near-bottom (50–54, 88–92) for ADCPs (1,2), respectively. In Tables 2 and 3, complex correlations which are larger than the significance level (0.44, Section 3) are in bold together with corresponding angular displacements. All three model runs coupled to NCOM CCS (with underestimated remote forcing) show correlations below the significance level.

Therefore, as long as the Monterey Bay model was coupled to NCOM CCS (with underestimated remote forcing), the increase in horizontal resolution or better representation of bathymetry did not raise the model versus observed currents correlation above the significance level. At the same time, coupling to HYCOM (with more accurate representation of the remote forcing) significantly increased the correlation between observed and model currents. For Run 4, with coarse resolution and smoothed bathymetry, correlations are higher than the significance level at all considered depths at ADCP2, and at the middle depth at ADCP1. The model Run 5 (with coarse resolution and unsmoothed bathymetry) performed the best: for all depths at ADCPs 1 and 2, correlations are higher than the significance level and angular displacements are not larger than 12°. Results in Tables 2 and 3 indicate that the most critical element in reproducing currents on the shelf is an accurate representation of the remote forcing in the form of the coastally-trapped Kelvin type waves. Comparisons of Runs 4 and 5 indicate that the second most important factor is an accurate representation of bathymetry. With unsmoothed bathymetry but the same horizontal resolution, Run 5 has a better correlation with observed currents than Run 4. Model Run 6 (with finer horizontal resolution than in Runs 4 and 5, and unsmoothed bathymetry as in Run 5), performed worse in comparison to Run 5 at ADCP1 and Run 4 at ADCP2.

Visual comparisons of observed and model-predicted currents are shown in Figs. 4 and 5. As indicated in Ramp et al. (2011), the observed currents at both ADCPs consisted of a strong poleward flow during 3–8 August. The event was nearly barotropic at both locations. This poleward flow coincides with the strong positive SSH anomalies in tide gauges data, and in HYCOM (Fig. 3). Runs 1–3, coupled to the NCOM CCS (that underestimates the poleward flow) shows weaker and more oriented inshore (positive values in U-component of velocity) poleward flow than in observations, especially at the ADCP2 location. Runs 4–6, coupled to HYCOM, captured the event in much better visual agreement with observations (Figs. 4 and 5). The best visual match in reproducing the strength and direction of this poleward flow is achieved by Run 5. In Run 6 (finer horizontal resolution than in Runs 4 and 5), the poleward flow is weaker and somewhat extended up to August 12 at ADCP2, especially below 20 m

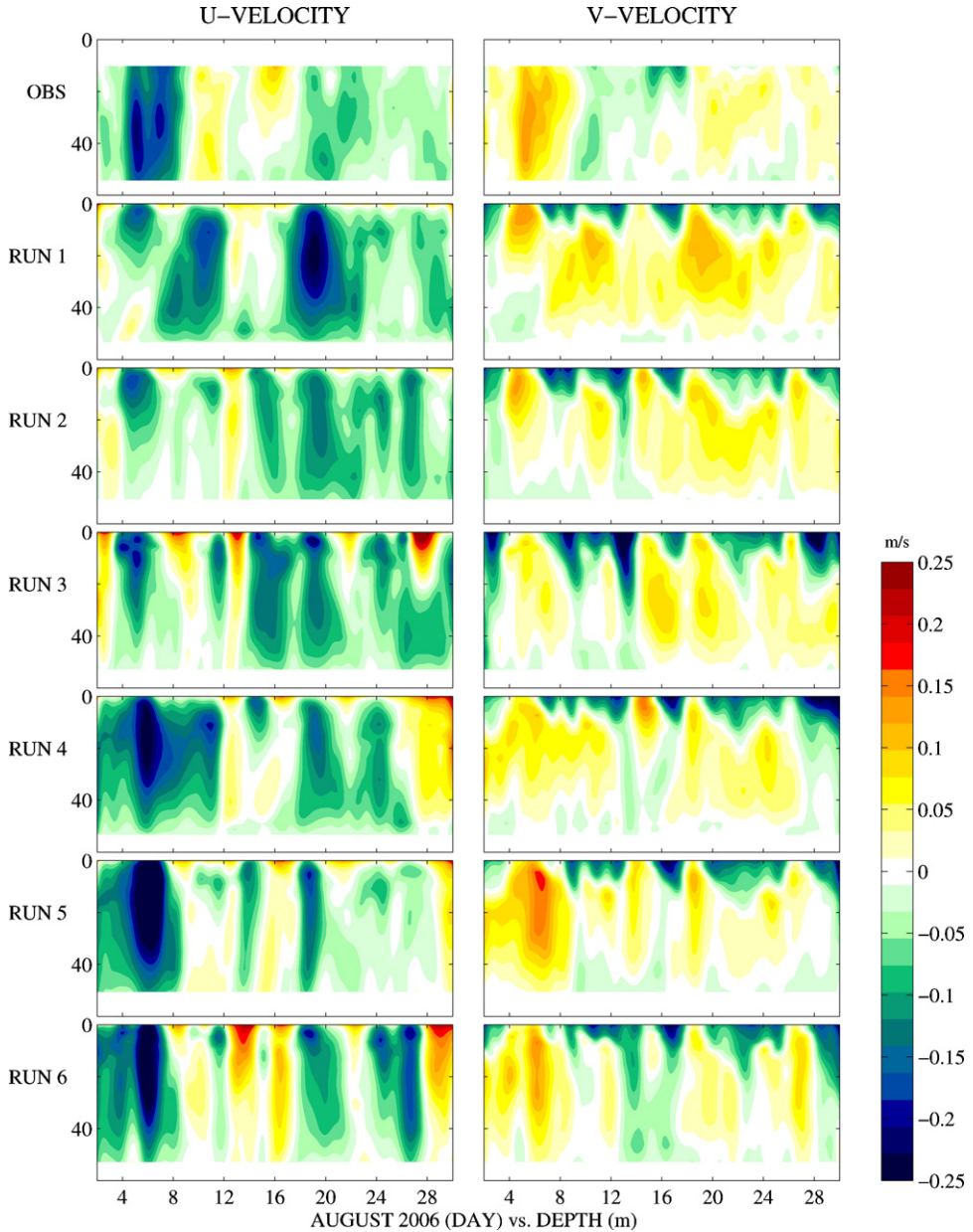


Fig. 4. Observed (top row) and model-predicted U (west–east, eastward flow is positive, left column) and V (south–north, northward flow is positive, right column) components of currents at ADCP1.

depth (Fig. 5). This is probably one of the reasons for low correlations (below the significant level) between Run 6 and ADCP2 currents (Table 3).

According to Ramp et al. (2011) and Figs. 4 and 5, the poleward flow was followed by an equatorward flow (during 9–17 August) at mooring locations. Run 5 reproduced this reversal best in timing and intensity (especially at ADCP2), while Run 6 shows a delay of the reversal below 20 m depth (almost 4

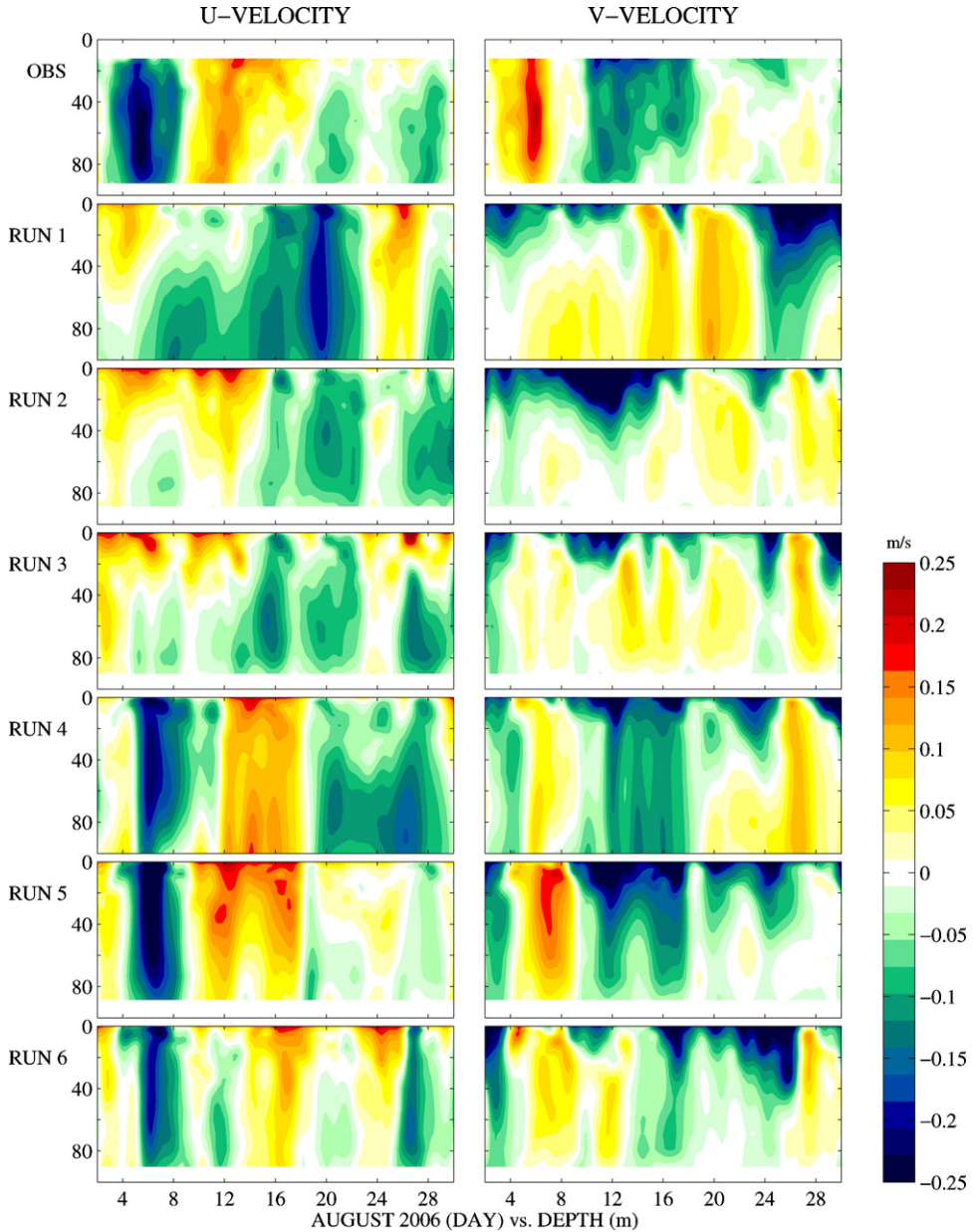


Fig. 5. Observed (top row) and model-predicted U (west–east, eastward flow is positive, left column) and V (south–north, northward flow is positive, right column) components of currents at ADCP2.

days delay). All Runs 1–3 (coupled to NCOM CCS) missed this transition from poleward to equatorward flow, especially at ADCP1.

For the remainder of the considered record (18–30 August), observations show a transition from equatorward flow to the weak poleward flow at ADCP1 and below 30 m depth at ADCP2. Model Runs 4–6 reproduced this weaker poleward flow in subsurface, while showing equatorward flow at surface

at ADCP1 (up to 10 m depth), and deeper (up to 40 m depth) at ADCP2. Run 6 shows a delay in currents reversal from equatorward to poleward.

5. Conclusions and discussions

Impacts of remote forcing, model resolution and bathymetry on currents predictions at two ADCP sites located on the shelf of the Monterey Bay area are investigated. The Monterey Bay area model configurations which differ in horizontal resolution, vertical grid and bathymetry representation (smoothed and unsmoothed) are used. Remote forcing (in the form of poleward propagating along the coast coastally-trapped Kelvin type waves) introduced through the coupling of the Monterey Bay model configurations to the larger scale models: the global HYCOM with accurate representation of remote forcing, and the regional California Current model (NCOM CCS) with underestimated remote forcing.

Comparisons of complex correlations and angular displacements between observed and model currents show that all model runs coupled to NCOM CCS (with underestimated remote forcing) show correlations below the significance level. At the same time, coupling to HYCOM (with accurate representation of the remote forcing) significantly increased the correlation between observed and model currents. Even the model run (Run 4 in Table 1) with coarse resolution and smoothed bathymetry showed higher than the significant level correlations at all considered depths at ADCP2, and at the middle depth at ADCP1. These results indicate that the most critical element in reproducing currents on the shelf is an accurate representation of the remote forcing in the form of the coastally-trapped Kelvin type waves. Also, comparisons of complex correlations have shown that an accurate representation of bathymetry is the second most critical factor to remote forcing in reproducing currents on the shelf.

Visual comparisons of observed and model-predicted currents support the above conclusions. Runs coupled with the HYCOM reproduced much better the intensity and direction of the observed strong poleward flow (3–8 August, Figs. 4 and 5). This poleward flow coincides with the strong positive SSH anomalies presented in tide gauges observations and the HYCOM (Fig. 3). Run 5, coupled to the HYCOM and with unsmoothed bathymetry, reproduced the best timing of the observed transition from the poleward flow to equatorward flow (observed during 9–17 August), and the transition back to the weak poleward flow for the remainder of the considered record (18–30 August).

As shown in Section 4, the impact of the horizontal resolution on the model predictions left mixed results. The model run with the finer horizontal resolution and unsmoothed bathymetry (Run 6, MBS3 model configuration) performed worse in comparison to the run with coarse resolution and unsmoothed bathymetry (Run 5, MBS2 model configuration) at both ADCP locations. Also, Run 6 demonstrated worse predictions at the ADCP2 location in comparison to Run 4 with coarser resolution and smoothed bathymetry (MBS1 model configuration). The decrease in predictive skill as we approach a very fine grid resolution might be the result of such factors as the deficiencies in physically based representation of dissipation rates, drag laws, sub-grid-scale parameterizations, truncation errors, as well as by approaching the limit of hydrostatic assumption. Another possible explanation might be the ratio of horizontal grid resolutions between the Monterey Bay model and the larger scale model. The HYCOM model resolution is around 9 km, while the MBS3 configuration has around 1–1.5 km resolution on open boundaries. This provides approximately 1 to 9 or 1 to 6 ratios in one way coupling on open boundaries. These high ratios of grid resolutions between larger scale versus local, finer resolution models in one way coupling probably introduce artificial time lags in propagating information from the larger scale model to the finer resolution Monterey Bay model (MBS3 configuration). This might introduce time lags in reproducing reversals from poleward to equatorward flows and back, which are discussed in Section 4. The above issues with the MBS3 configuration are planned to be investigated in our future research.

Acknowledgments

This research was funded through the Naval Research Laboratory (NRL). Computer time for the numerical simulations was provided through a grant from the Department of Defense High Performance Computing Initiative. This manuscript is NRL contribution: 7330-12-1514.

References

- Barron, C.N., Kara, A.B., Hurlburt, H.E., Rowley, C., Smedstad, L.F., 2004. Sea surface height predictions from the Global Navy Coastal Ocean Model (NCOM) during 1998–2001. *J. Atmos. Oceanic Technol.* 21, 1876–1894.
- Beardsley, R., Limeburner, C.R., Rosenfeld, L.K., 1985. WHOI Tech. Rep., pp. 35–85.
- Chassignet, E.P., Hurlburt, H.E., Metzger, E.J., Smedstad, O.M., Cummings, J., Halliwell, G.R., Bleck, R., Baraille, R., Wallcraft, A.J., Lozano, C., Tolman, H.L., Srinivasan, A., Hankin, S., Cornillon, P., Weisberg, R., Barth, A., He, R., Werner, F., Wilkin, J., 2009. U.S. GODAE: Global Ocean Prediction with the HYbrid Coordinate Ocean Model (HYCOM). *Oceanography* 22 (2), 64–75.
- Chelton, D.B., Davis, R.E., 1982. Monthly mean sea level variability along the west coast of North America. *J. Phys. Oceanogr.* 12, 757–784.
- Cummings, J., Bertino, L., Brasseur, P., Fukumori, I., Kamachi, M., Martin, M.J., Mogensen, K., Oke, P., Testud, C.E., Verron, J., Weaver, A., 2009. Ocean data assimilation systems for GODAE. *Oceanography* 22 (3), 96–109.
- Cummings, J.A., 2005. Operational multivariate ocean data assimilation. *Q. J. R. Meteorol. Soc.* 131, 3583–3604, <http://dx.doi.org/10.1256/qj.05.105>.
- Denbo, D.W., Allen, J.S., 1987. Large-scale response to atmospheric forcing of shelf currents and coastal sea level off the west coast of North America: May–July 1981 and 1982. *J. Geophys. Res.* 92, 1757–1782.
- Doyle, J.D., Jiang, Q., Chao, Y., Farrara, J., 2009. High-resolution real-time modeling of the marine atmospheric boundary layer in support of the AOSN-II field campaign. *Deep Sea Res. Part II* 56, 87–99.
- Flather, R.A., 1976. A tidal model of the northwest European continental shelf. *Memorie Soc. Real Sci.* 6, 141–164.
- Fox, D.N., Barron, C.N., Carnes, M.R., Booda, M., Peggion, G., Van Gurley, J., 2002. The modular ocean data assimilation system. *Oceanography* 15 (1), 22–28.
- Haney, R.L., 1991. On the pressure gradient force over steep topography in sigma coordinate ocean models. *J. Phys. Oceanogr.* 21, 610–619.
- Kundu, P.K., 1976. Ekman veering observed near the ocean bottom. *J. Phys. Oceanogr.* 6, 238–242.
- Leonard, N.E., Paley, D.A., Davis, R.E., Fratantoni, D.M., Lekien, F., Zhang, F., 2010. Coordinated control of an underwater glider fleet in an adaptive ocean sampling field experiment in Monterey Bay. *J. Field Robotics* 27, 718–740.
- Martin, P. J. (2000). Description of the Navy Coastal Ocean Model version 1.0. Rep. NRL/FR/732-00-9962, Nav. Res. Lab., Stennis Space Center, Mississippi.
- Metzger, E.J., Hurlburt, H.E., Xu, X., Shriver, J.F., Gordon, A.L., Sprintall, J., Susanto, R.D., van Aken, H.M., 2010. Simulated and observed circulation in the Indonesian Seas: 1/12° global HYCOM and the INSTANT observations. *Dyn. Atmos. Oceans* 50, 275–300.
- Ramp, S.R., Lermusiaux, P.F.J., Shulman, I., Chao, Y., Wolf, R.E., Bahr, F.L., 2011. Oceanographic and atmospheric conditions on the continental Shelf North of the Monterey Bay during August 2006. *Dyn. Atmos. Oceans* 52, 192–223.
- Rhodes, R.C., Hurlburt, H.E., Wallcraft, A.J., Barron, C.N., Martin, P.J., Smedstad, O.M., Cross, S., Metzger, J.E., Shriver, J., Kara, A., Ko, D.S., 2002. Navy real-time global modeling systems. *Oceanography* 15 (1), 29–43.
- Rosmond, T.E., Teixeira, J., Peng, M., Hogan, T.F., Pauley, R., 2002. Navy Operational Global Atmospheric Prediction System (NOGAPS): forcing for ocean models. *Oceanography* 15, 99–108.
- Shulman, I., Anderson, S., Rowley, C., DeRada, S., Doyle, J., Ramp, S., 2010. Comparisons of upwelling and relaxation events in the Monterey Bay area. *J. Geophys. Res.* 115, C06016, <http://dx.doi.org/10.1029/2009JC005483>.
- Shulman, I., Kindle, J., Martin, P., deRada, S., Doyle, J., Penta, B., Anderson, S., Chavez, F., Paduan, J., Ramp, S., 2007. Modeling of upwelling/relaxation events with the Navy Coastal Ocean Model. *J. Geophys. Res.* 112, C06023, <http://dx.doi.org/10.1029/2006JC003946>.
- Spillane, M.C., Enfield, D.B., Allen, J.S., 1987. Intraseasonal oscillations in sea level along the west coast of the Americas. *J. Phys. Oceanogr.* 17, 313–325.
- Wilks, D.S., 1995. *Statistical Methods in the Atmospheric Sciences*. Academic, San Diego 467.
- Zamudio, L., Hogan, P.J., Metzger, E.J., 2008. Summer generation of the southern Gulf of California eddy train. *J. Geophys. Res.* 113, C06020, <http://dx.doi.org/10.1029/2007JC004467>.
- Zamudio, L., Hogan, P.J., Metzger, E.J., 2011. Modeling the seasonal and interannual variability of the northern Gulf of California salinity. *J. Geophys. Res.* 116, C02017, <http://dx.doi.org/10.1029/2010JC006631>.